Journal of Alloys and Compounds 499 (2010) 98–103

Contents lists available at ScienceDirect

Journal of Alloys and Compounds

journal homepage: www.elsevier.com/locate/jallcom

Synthesis and characterization of novel conductive and magnetic nano-composites

A.A. Farghali, M. Moussa, M.H. Khedr*

Materials Science Laboratory, Chemistry Department, Faculty of Science, Beni-Suef University, Egypt

ARTICLE INFO

Article history:
Received 25 November 2009
Received in revised form 11 March 2010
Accepted 13 March 2010
Available online 19 March 2010

Keywords:
Nano-composite
Polyaniline
Cobalt magnesium ferrite
Core-shell
Magnetic and electrical properties
Dye adsorption

ABSTRACT

In the last years, a great deal of attention has been paid to use nano-sized ferrites as advanced additives in conducting polymers. The embedding of the ferrite materials into polymeric matrices is the simplest way to take advantage of some novel physical characteristics. In the present work, the preparation of a polyaniline/$Co_{1-x}Mg_xFe_2O_4$ nano-composite ($x = 0, 0.5, 1$) with good magnetic and electrical properties was described. The structure, morphologies and properties of the samples were characterized by XRD, FT-IR, TEM, TGA, VSM and conductivity measurements. Nano-particles appear well dispersed in the polymer matrix and the results of TGA indicated that the ferrite nano-particles could improve the composite thermal stability. The electrical conductivity of the pure polyaniline decreased while the saturation magnetization (M_s) and coercivity (H_c) increased with ferrite. The ability of the composites to remove the toxic dyes from waste water was investigated.

1. Introduction

Polymer nano-composites synthesis is a hybridization process between polymer matrices and nano-particles. The main idea in a composite is to integrate several component materials and their properties in a single material. As a result, considerable efforts currently have been directed by many researchers towards the conducting polymer nano-composites because of their unique properties, as well as their well applicable multi-functionality in various fields [1]. Polyaniline (PANI) is a conducting polymer so it has many potential applications in various fields such as electrical-magnetic shields, microwave absorbing materials, batteries, sensors and corrosion protections [2–10]. The development of the PANI properties has received considerable attention lately. The fabrication of PANI/ferrite nano-composite has been reported by using different methods such as in situ polymerization of aniline in the presence of $Zn_{0.6}Cu_{0.4}Cr_{0.5}Fe_{1.5}O_4$ nano-particles [11], micro-emulsion process used to prepare PANI/NiZn ferrite nano-composite [12] and oxidative electro-polymerization of aniline in an aqueous solution in the presence of MnZn ferrite and NiMnZn ferrite [13], these studies created organic materials possessing both conducting and ferromagnetic functions.

The electromagnetic measurements of the PANI/ferrites were improved and tailored by controlling the addition of the ferrite in the composite [14,15]. Also, the contribution of ferrite to the PANI led to an increase in its thermal stability, however, it decreased its electrical conductivity [16–18]. Jiang et al. introduced a novel poly(aniline-co-o-toluidine)/$BaFe_{12}O_{19}$ composite [19], which was successfully synthesized by a facile, general and inexpensive in situ polymerization method. Ting et al. had reported the microwave absorption of the PANI/$BaFe_{12}O_{19}$ [20] and noticed that Microwave absorbing properties can be modulated simply by controlling the content of PANI on the samples for the required frequency bands. Another new routes for synthesizing the PANI nano-composites, hollow Fe_3O_4–PANI spheres with uniform cavity size and shell thickness suggested [21], PANI nanotubes containing Fe_3O_4 nano-particles synthesized under ultrasonic irradiation [22] where the Fe_3O_4 nano-particles embedded in PANI nanotubes. The PANI nano-composites focus not only on ferrites but they extended to other materials such as titanium dioxide, zinc oxide, manganese oxide, vanadium pentaoxide, clinoptilolite, nafion, carbon nanotubes and silicon [23–30].

In this work, an approach was reported to synthesize the PANI/$Co_{1-x}Mg_xFe_2O_4$ nano-composites ($x = 0, 0.5, 1$) by in situ polymerization of aniline with $Co_{1-x}Mg_xFe_2O_4$ particles. The obtained composite was characterized by various experimental techniques. The removal of the pollutants from waste water by using the PANI/ferrite nano-composites was investigated. The electrical conductivity of the pure polyaniline, the saturation magnetization (M_s) and coercivity (H_c) were measured and found to be affected dramatically with ferrite addition. The ability of the composites to remove the toxic dyes from waste water was also investigated.

* Corresponding author. Tel.: +20 105200230.
E-mail address: dkhedr@yahoo.com (M.H. Khedr).

0925-8388/$ – see front matter © 2010 Published by Elsevier B.V.
doi:10.1016/j.jallcom.2010.03.124

2. Experimental

2.1. Preparation of $Co_{1-x}Mg_xFe_2O_4$

$Co_{1-x}Mg_xFe_2O_4$ (x = 0, 0.5, 1) nano-particles were prepared by mixing a solution of $Co(NO_3)_2{\cdot}6H_2O$, $Mg(NO_3)_2{\cdot}6H_2O$ and $Fe(NO_3)_3{\cdot}9H_2O$ in stoichiometric ratio with a solution containing NaOH + Na_2CO_3 [31,32] ([NaOH] = 1.6[Mg^{2+} + Co^{2+} + Fe^{3+}], [CO_3^{2-}] = 2.0[Fe^{3+}]) in de-ionized water (pH ≈ 9). The solutions simultaneously added to a colloid mill [33,34] and mixed for 2 min. The resulting slurry was placed in a three neck flask and aged at 100 °C for 6 h. The final precipitate was filtered, washed thoroughly with de-ionized water and dried at 100 °C for 24 h. The resulting sample was then calcined at 900 °C for 2 h and then grinded to obtain a fine powder.

2.2. Synthesis of PANI/$Co_{1-x}Mg_xFe_2O_4$

A typical in situ chemical polymerization method for the PANI/$Co_{1-x}Mg_xFe_2O_4$ was carried out by the routine synthesis [17]. 0.5 g of $Co_{1-x}Mg_xFe_2O_4$ was added to 50 ml of freshly prepared reaction mixture (0.2 M aniline and 0.25 M ammonium peroxydisulphate in 1 M HCl) at 20 °C. The mixture was stirred during the polymerization of aniline for 12 h. The ferrite coated with PANI was separated on a filter paper, rinsed with 1 M HCl and warm de-ionized water, and dried at 70 °C in an electrical oven.

2.3. Sample analysis

The $Co_{1-x}Mg_xFe_2O_4$, PANI and PANI/$Co_{1-x}Mg_xFe_2O_4$ NC were identified by X-ray diffraction technique JSX-60P JEOL diffractometer. The average crystallite size was calculated using software TOPAZ 2 through the diffractions peaks from Scherer's formula [35] as shown below:

$$D = \frac{0.9\lambda}{\beta \cos\theta}$$

where D is the crystal size, λ is the X-ray wave length, β is the broadening of the diffraction peak and θ is the diffraction angle. The FT-IR spectra measured using FT/IR JASCO 6100. Morphology of the nano-composite was observed using TEM (JEOL JEM-1230) and reflected light microscopy (Meiji-CK3900 reflected light microscope with video camera), the magnetic properties were investigated by Vibrating Sample Magnetometer model 9600 while the thermal analysis was performed using MAC-science model DTA-TG2000. UV–vis spectra of the samples dissolved in N,N-dimethylformamide (DMF) and the adsorption rate of the bromopyrogallol red dye on the samples were recorded with JASCO V-530 UV–vis Spectrophotometer. The electrical measurements were performed by using computerized avometer BK precision 390A, powder is compressed at 6 tons to pellets and coated by silver past.

3. Results and discussion

3.1. X-ray diffraction

3.1.1. X-ray diffraction of $Co_{1-x}Mg_xFe_2O_4$

The room temperature powder XRD patterns of as-prepared $Co_{1-x}Mg_xFe_2O_4$ ferrite particles are shown in Fig. 1. The well resolved broad diffraction peaks corresponding to (2 2 0), (3 1 1), (2 2 2), (4 0 0), (4 2 2), (5 1 1) and (4 4 0) reflection planes show that all the ferrites have attained single phase, all the peaks can be indexed to a single phase spinel structure. The crystal sizes (L) of the $Co_{1-x}Mg_xFe_2O_4$ ferrite are 115, 94 and 33 nm for x = 0, 0.5 and 1, respectively. The values of lattice parameters of the ferrites as described by Ahmed and El-khawlani [36] decrease with the increasing concentration of Mg^{2+} and the grain size also shows a similar trend. The decreasing trend in the lattice parameter values is due to the smaller Mg^{2+} ion (0.72 Å) replacing the larger Co^{2+} ion (0.745 Å). Also, the X-ray density decreases with Mg^{2+} concentration because the decrease in mass overcomes the decrease in volume of the unit cell. On the other hand this may be due to the difference in atomic weight of the Co^{2+} and Mg^{2+} ions (58.933 and 24.312 amu), respectively [36].

3.1.2. X-ray diffraction of PANI/$Co_{0.5}Mg_{0.5}Fe_2O_4$

Fig. 2(a–c) shows the XRD pattern of PANI/$Co_{0.5}Mg_{0.5}Fe_2O_4$ NC. It is observed that the two broad diffraction peaks centered at 2θ values of 20.1° and 25.3° are the characteristic peaks of the doped PANI (Fig. 2a), which can be ascribed to the periodicity parallel and perpendicular to the polymer chains, respectively [37]. The diffraction pattern for PANI/$Co_{0.5}Mg_{0.5}Fe_2O_4$ composite is shown in Fig. 2c. It shows the characteristic peaks of $Co_{0.5}Mg_{0.5}Fe_2O_4$ as well as the broad diffraction peaks of PANI. The peaks intensities for PANI/$Co_{0.5}Mg_{0.5}Fe_2O_4$ NC become weaker than that for the pure $Co_{0.5}Mg_{0.5}Fe_2O_4$, which reveals that the PANI coating layer (shell) affects the crystalline structure of $Co_{0.5}Mg_{0.5}Fe_2O_4$.

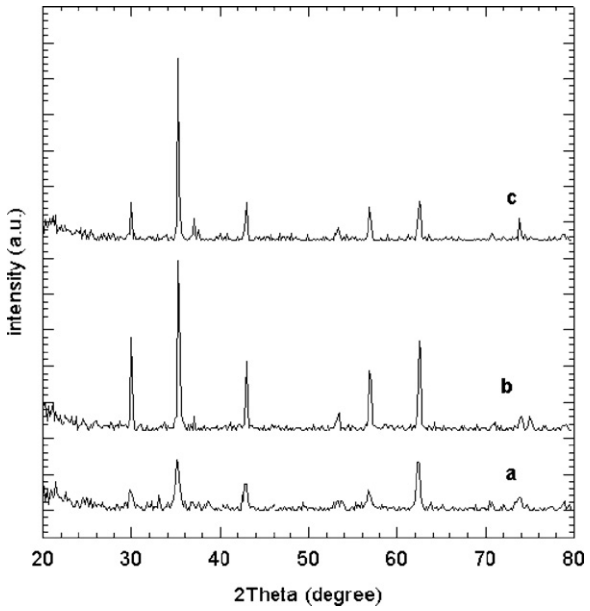

Fig. 1. X-ray diffraction pattern of $MgFe_2O_4$ (a), $Co_{0.5}Mg_{0.5}Fe_2O_4$ (b) and $CoFe_2O_4$ (c).

3.2. FT-IR spectra

Fig. 3 compares the FT-IR absorption spectra of PANI and PANI/$Co_{1-x}Mg_xFe_2O_4$ NC. The main characteristic peaks of the PANI are assigned as follow: The bands at 1558 and 1471 cm^{-1} are the characteristic C=C stretching of the quinoid and benzonoid rings while the bands observed at 1294 and 787 cm^{-1} may be assigned to the C–N stretching of the secondary aromatic amine and an aromatic C–H out-of-plane bending vibration, respectively. The rel-

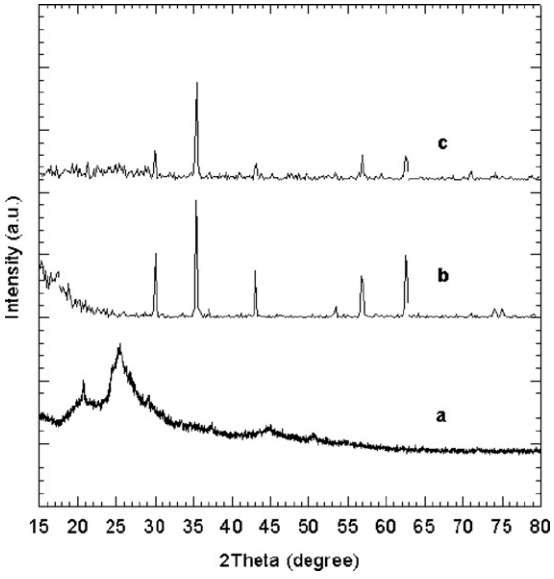

Fig. 2. XRD pattern of PANI (a), $Co_{0.5}Mg_{0.5}Fe_2O_4$ (b) and PANI/$Co_{0.5}Mg_{0.5}Fe_2O_4$ (c).

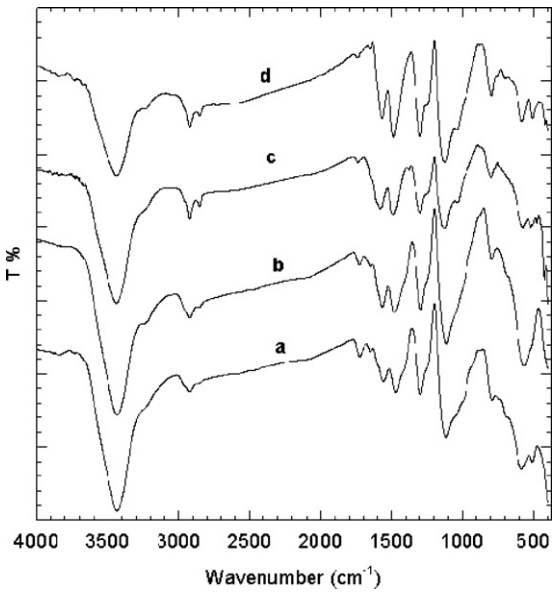

Fig. 3. FT-IR spectra of PANI (a), PANI/$MgFe_2O_4$ (b), PANI/$Co_{0.5}Mg_{0.5}Fe_2O_4$ (c) and PANI/$CoFe_2O_4$ (d).

atively small peak observed at 3432 cm^{-1} may be attributed to the N–H stretching vibration mode. In the region of 1010–1170 cm^{-1} aromatic C–H in-plane bending modes were usually observed. In addition, the peak at 2922 cm^{-1} resulted from cross-linking moieties [38]. The IR spectra of PANI/$Co_{1-x}Mg_xFe_2O_4$ NC (Fig. 3b–d) are almost identical to that of PANI, due to the higher mass of the participating atoms, vibrations of transitional metal-oxygen bonds appear in the far-infrared region (Table 1) [11].

3.3. TEM

The nano-particles of $Co_{1-x}Mg_xFe_2O_4$ and modified PANI/$Co_{1-x}Mg_xFe_2O_4$ are revealed by the TEM image (Fig. 4), from which it was found that PANI/$Co_{1-x}Mg_xFe_2O_4$ do not change the size of $Co_{1-x}Mg_xFe_2O_4$ significantly, as shown in Fig. 4(a)–(c), and the crystal sizes of the samples are in agreement with that obtained from XRD patterns. TEM images (Fig. 4) show also that the ferrite particles are embedded in the PANI matrix forming the core-shell structure, the dark core is the ferrite particles, and the light colored shell is the PANI as a result of the different electron penetrability.

3.4. TGA measurements

The composition of PANI/$Co_{0.5}Mg_{0.5}Fe_2O_4$ composite can be analyzed from TGA. Fig. 5 shows the TGA and DTG curves for a pure PANI and PANI/$Co_{0.5}Mg_{0.5}Fe_2O_4$. The pure PANI undergoes three weight loss steps. The first step indicates a weight loss at a temperature up to 120 °C which may be attributed to the expulsion of water molecule and the dopant (HCl) from PANI chains. The sec-

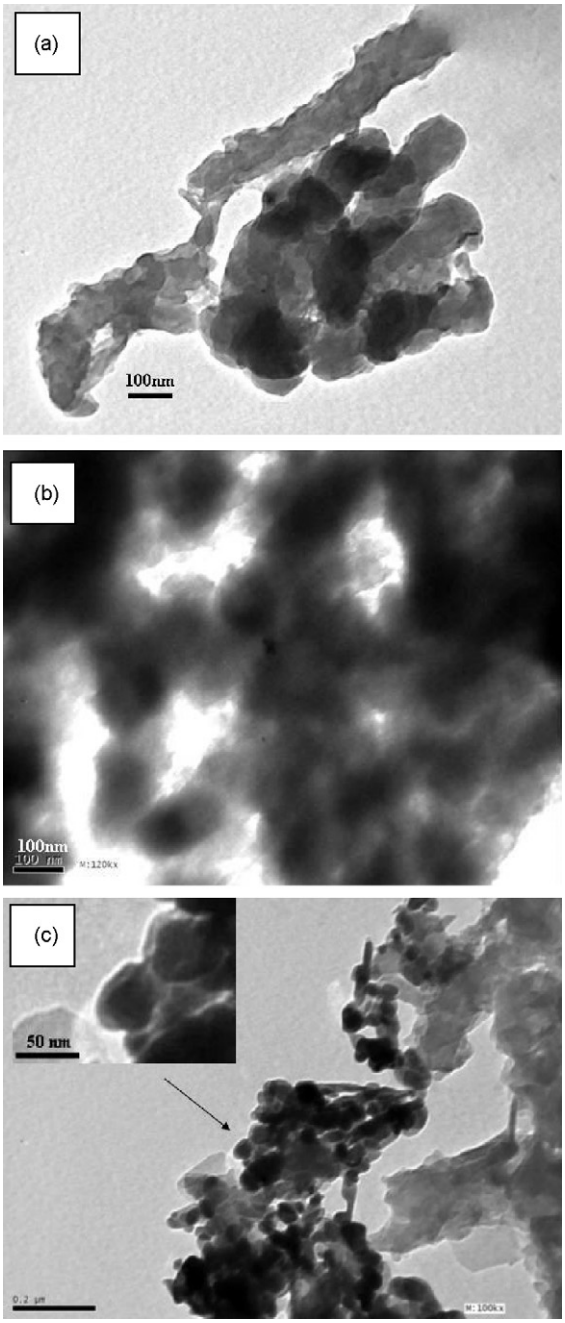

Fig. 4. TEM images of PANI/$CoFe_2O_4$ (a), PANI/$Co_{0.5}Mg_{0.5}Fe_2O_4$ (b) and PANI/$MgFe_2O_4$ (c).

Table 1
FT-IR absorption peaks for PANI and PANI/$Co_{1-x}Mg_xFe_2O_4$.

Peak assignment	Wavenumber (cm^{-1})			
	PANI	PANI/$CoFe_2O_4$	PANI/$Co_{0.5}Mg_{0.5}Fe_2O_4$	PANI/$MgFe_2O_4$
N–H stretching vibration	3432	3436	3436	3432
Cross-linking moieties	2922	2922	2922	2922
Quinoid ring stretching	1558	1566	1579	1564
Benzenoid ring stretching	1471	1486	1490	1480
Aromatic C–N stretching	1294	1297	1295	1294
C–H out-of-plane bending vibration	787	795	797	794

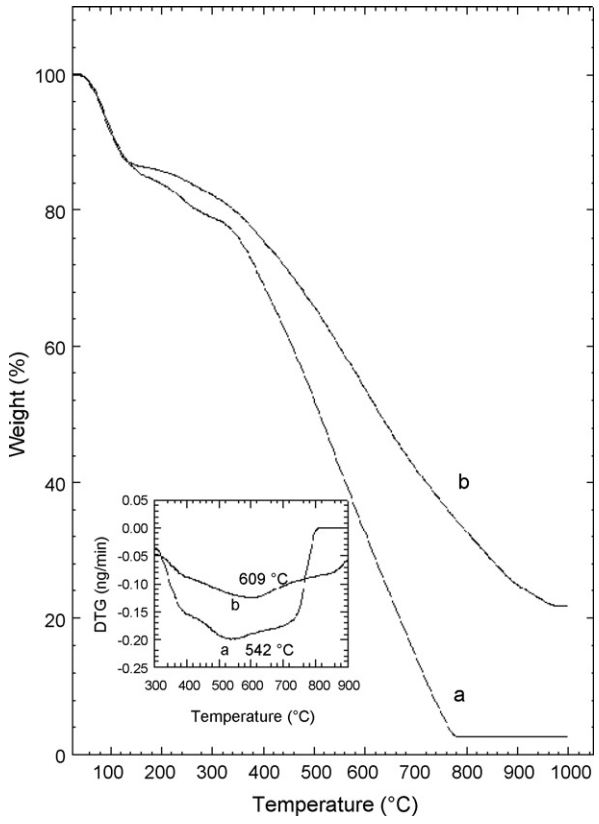

Fig. 5. TGA and DTG curves of PANI (a) and PANI/$Co_{0.5}Mg_{0.5}Fe_2O_4$ (b).

ond step is observed in the temperature range of 200–350 °C which may be due to the volatilization of lower weight PANI. The final step at higher temperatures may be due to the thermal degradation of PANI chains. As revealed from Fig. 5, the thermal stability of the composite is higher than that of pure PANI. For instance, the TGA curve of the PANI/$Co_{0.5}Mg_{0.5}Fe_2O_4$ composite reveals a weight loss of 50% at 629.1 °C. In contrast, the pure PANI shows the same weight loss at 510.5 °C. Also in the inserted DTG curves the temperature of pure PANI at the minimum of the DTG curve is at 542.12 °C, but the minimum temperature in the case of the PANI/$Co_{0.5}Mg_{0.5}Fe_2O_4$ NC is significantly shifted to higher temperature by about 67 °C. This would be explained by the fact that a strong interaction between PANI and $Co_{0.5}Mg_{0.5}Fe_2O_4$ restricts thermal motion of the PANI in the composite and enhances a thermal stability of the composite [39].

3.5. Magnetic properties

Fig. 6 shows the magnetization, *M*, versus the applied magnetic field, *H*, for $Co_{1-x}Mg_xFe_2O_4$ at room temperature. The magnetization of $Co_{1-x}Mg_xFe_2O_4$ exhibits a clear hysteretic behavior. Table 2 gives the magnetic parameters such as saturation magnetization

Table 2
Magnetic parameters of PANI, $Co_{1-x}Mg_xFe_2O_4$and PANI/$Co_{1-x}Mg_xFe_2O_4$.

Sample	M_s (emu/g)	M_r (emu/g)	H_c (Oe)
PANI	0.0463	0.01051	18.97
$CoFe_2O_4$	81.94	38.09	678
PANI/$CoFe_2O_4$	19.08	7.634	688.9
$MgFe_2O_4$	21.33	2.108	88.66
PANI/$MgFe_2O_4$	5.905	0.6659	81.6
$Co_{0.5}Mg_{0.5}Fe_2O_4$	54.18	27.51	649.5
PANI/$Co_{0.5}Mg_{0.5}Fe_2O_4$	13.67	6.806	640

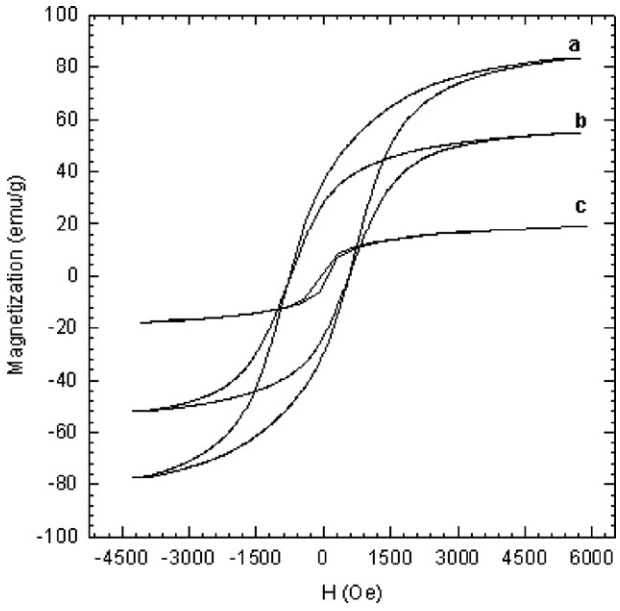

Fig. 6. Hysteretic loops of $CoFe_2O_4$ (a), $Co_{0.5}Mg_{0.5}Fe_2O_4$ (b) and $MgFe_2O_4$ (c).

(M_s), coercivity (H_c) and remnant magnetization (M_r) that determined by hysteresis loops measurement. We can observe that the values M_s, M_r and H_c for $Co_{1-x}Mg_xFe_2O_4$ decrease with Mg^{2+} concentrations, this is attributed to that Co^{2+} and Mg^{2+} ions have a strong preference to occupy the B-sites, it is known that the magnetic moment of Co^{2+} in spinel ferrite is 3 μB [40]; however, the magnetic moment of Mg^{2+} is zero. Since both of these ions occupy the octahedral sites, thus the subsequent substitution of Co^{2+} ions by non-magnetic Mg^{2+} ions is expected to decrease the saturation magnetization and the net magnetic moment.

It is observe that the values M_s, M_r and H_c for PANI/$Co_{1-x}Mg_xFe_2O_4$ NC (Fig. 7) have the same order in pure $Co_{1-x}Mg_xFe_2O_4$ with Mg^{2+} concentrations as above but, these values for the composites are less than those obtained for pure $Co_{1-x}Mg_xFe_2O_4$, this behavior is due to the non-magnetic coating

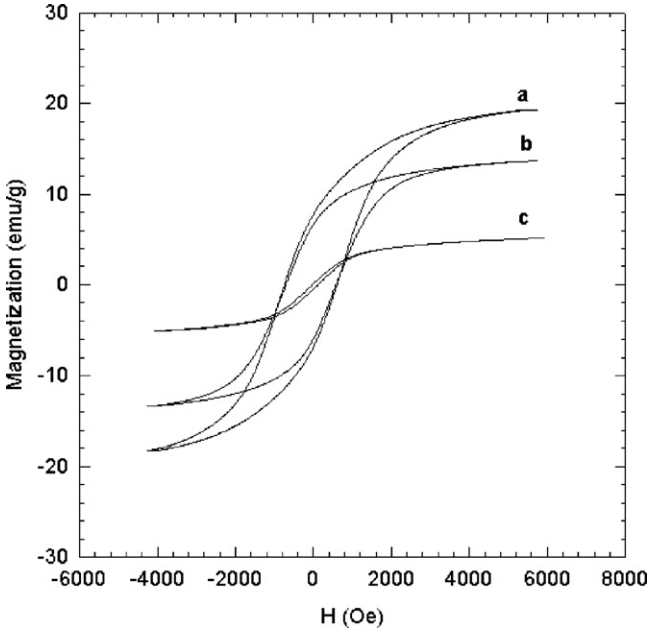

Fig. 7. Hysteretic loops of PANI/$CoFe_2O_4$ (a), PANI/$Co_{0.5}Mg_{0.5}Fe_2O_4$ (b) and PANI/$MgFe_2O_4$ (c).

layer, can be envisaged as a magnetic dead layer on the surface, thus affecting the magnitude of magnetization due to quenching of the surface moment [41] and also, according to the equation $M_s = \varphi m_S$, where (φ) is the volume fraction of the particles and (m_S) is the saturation moment of a single particle, it is clear that Ms of the composite is dependent on the volume fraction of the magnetic ferrite particles (φ), and hence, due to the contribution of the non-magnetic PANI coating layer to the total magnetization, the PANI/$Co_{1-x}Mg_xFe_2O_4$ NC has less magnetization than that observed for the pure cobalt magnesium ferrite nano-particles.

The coercivity is dependent on surface anisotropy and interparticle interactions so, the coating of the ferrite by PANI will affect on the participation of these anisotropy mechanisms to the net anisotropy (K) [42]. K_s results from low coordination symmetry for spin-orbit couplings at the surface of nano-particles and contributes to K:

$$K = K_b + \left(\frac{6}{d}\right) K_s \quad (1)$$

where K_b is the bulk anisotropy and d is the particle diameter. K_s is usually maximum for free surfaces and is reduced by solid coverage.

According to the Stoner–Wohlfarth theory, H_c of a single domain particle is proportionally related to the anisotropy:

$$H_c = \left(\frac{2K}{\mu_0 M_s}\right) \quad (2)$$

where μ_0 is the permeability of the vacuum. The decrease in K_s resulting from the particle coverage by the PANI shell reduces the effective magnetocrystalline anisotropy (K) and therefore decreases H_c.

3.6. Electrical measurements

The presence of $Co_{1-x}Mg_xFe_2O_4$ nano-particles significantly affects the conductivity of the resulting composite, the conductivity of pure PANI was reduced from 5.7×10^{-2} to 4.2×10^{-2} S/cm, 2.7×10^{-2} and 3.4×10^{-2} S/cm for PANI/$Co_{1-x}Mg_xFe_2O_4$ (x = 0, 0.5, 1), respectively. This behavior is due to: (1) the $Co_{1-x}Mg_xFe_2O_4$ nano-particles are embedded in the PANI matrix, thus the interaction between the polymer matrix and iron oxide nano-particles will increase the charge carrier scattering and thus decreases the conductivity of the sample; (2) an increase of the charge carrier trapping, either by the nano-particles themselves or by morphological changes and defects induced by them [43]; (3) a decrease of the doping degree [12]. The values of the measured conductivity proved that there was an interaction between $Co_{1-x}Mg_xFe_2O_4$ and PANI backbone.

3.7. Dye removal from waste water by using PANI and its composites

The effect of $Co_{1-x}Mg_xFe_2O_4$ on PANI in the adsorption of bromopyrogallol red (BPR) as sulfonate and toxic dye was investigated, The UV–vis spectra of (BPR) is represented by Fig. 8 that indicates two characteristic wavelengths for BPR, one in visible light region at 555 nm and the other in UV region at 282 nm. The adsorption reaction is followed by the change of the concentration of BPR at 555 nm. As reported mechanism [44], when [BPR.]–SO_3H is dissolved in water, it dissociated to anionic form bearing –SO_3^- group which is adsorbed by chemical interaction with the positively charged backbone of PANI emeraldine salt, and H^+ ions interact with the chloride ions that are invariably present in doped PANI.

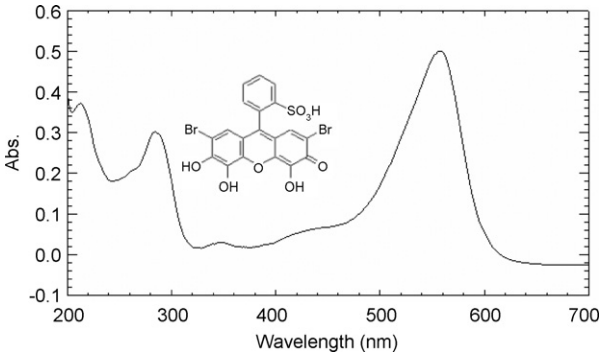

Fig. 8. UV–vis spectra of bromopyrogallol red dye.

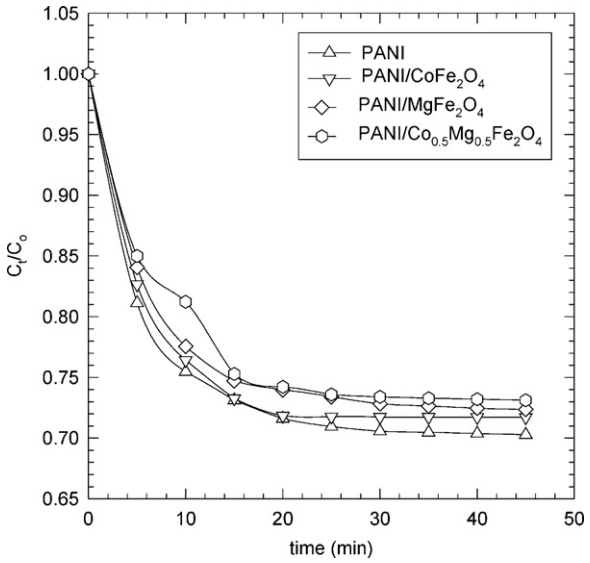

Fig. 9. Adsorption of bromopyrogallol red dye 4 ppm at different time intervals of PANI and its composites.

The concentration change of BPR with time in case of PANI, PANI/$Co_{1-x}Mg_xFe_2O_4$ and $Co_{1-x}Mg_xFe_2O_4$is shown in Fig. 9 where C_o is the initial concentration and C_t is the concentration at time t which indicates that the rapid uptake of the dye by PANI is more than that of PANI/$Co_{1-x}Mg_xFe_2O_4$. A second-order model for adsorption indicates [44,45]

$$\frac{t}{q_t} = \frac{1}{k_s q_e^2} + \frac{1}{q_e} t \quad (3)$$

where q_e is the amount adsorbed at equilibrium, k_s is the rate constant in mg of PANI/[(mg of dye)min] and q_t is the amount adsorbed at time t in mg of dye/mg of PANI. Thus, a plot of t/q_t versus t should be linear for various composites. The values of $k_s q_e^2$ and q_e, determined from the slope and intercept of the plot, respec-

Table 3
Kinetic parameters for the adsorption of BPR on PANI and PANI/$Co_{1-x}Mg_xFe_2O_4$.

Sample	q_e (mg of dye/mg of PANI)	$k_s q_e^2$ {mg of dye/[(mg of PANI)min]}
PANI	0.5225	0.1799
PANI/$CoFe_2O_4$	0.4965	0.1786
PANI/$MgFe_2O_4$	0.4916	0.1423
PANI/$Co_{0.5}Mg_{0.5}Fe_2O_4$	0.4908	0.1133

tively, are reported in Table 3, these values indicate that the k_s and q_e of PANI are higher than that of PANI/$Co_{1-x}Mg_xFe_2O_4$. From the above data, it is clear that the presence of $Co_{1-x}Mg_xFe_2O_4$ with PANI affected its adsorption rate to BPR. This behavior is due to the doping degree in PANI is greater than PANI/$Co_{1-x}Mg_xFe_2O_4$and as described, the role of the dopant in adsorption mechanism, the positively charged backbone and chloride ions (active sites) that are invariably present in the emeraldine salt are lower in PANI/$Co_{1-x}Mg_xFe_2O_4$ than PANI leading to the adsorption rate of the composite to be slightly lower than that of PANI. Also, it is noted that the rate of adsorption on the composites in the order PANI/$CoFe_2O_4$ > PANI/$MgFe_2O_4$ > PANI/$Co_{0.5}Mg_{0.5}Fe_2O_4$, which reflects the degree of doping (conductivity).

4. Conclusions

The pure PANI and PANI/$Co_{1-x}Mg_xFe_2O_4$ (x = 0, 0.5, 1) composites have been prepared by chemical oxidative method in the presence of aniline and $Co_{1-x}Mg_xFe_2O_4$ by ammonium peroxydisulphate oxidant in HCl medium. The obtained data shows that there is an interaction between the ferrite and PANI in the obtained composites which have core-shell structure, the presence of the ferrites with the PANI increases the thermal stability of the PANI. The magnetic properties of PANI were improved by adding the ferrites, the variation in the saturation of magnetization (M_s) for $Co_{1-x}Mg_xFe_2O_4$ (x = 0, 0.5, 1) facilitated the production of composite materials with considerable properties. The conductivity of the nano-composites was found to be decreased by adding the ferrite. The adsorption of bromopyrogallol red dye (BPR) on the PANI was investigated and the adsorption rate was affected by presence of $Co_{1-x}Mg_xFe_2O_4$.

References

[1] P.M. Dziewoński, M. Grzeszczuk, Electrochim. Acta 55 (2010) 3336.
[2] S. Bhadra, N.K. Singha, D. Khastgir, Curr. Appl. Phys. 9 (2009) 396.
[3] S.V. Jadhav, V. Puri, Microelectron. J. 39 (2008) 1472.
[4] K. Lakshmi, H. John, K.T. Mathew, R. Joseph, K.E. George, Acta Mater. 57 (2009) 371.
[5] A.I. Gopalan, P. Santhosh, K.M. Manesh, J.H. Nho, S.H. Kim, C.-G. Hwang, K.-P. Lee, J. Membr. Sci. 325 (2008) 683.
[6] K. Crowley, A. Morrin, A. Hernandez, E. O'Malley, P.G. Whitten, G.G. Wallace, M.R. Smyth, A.J. Killard, Talanta 77 (2008) 710.
[7] A. Airoudj, D. Debarnot, B. Bêche, F. Poncin-Epaillard, Anal. Chim. Acta 626 (2008) 44.
[8] A. Airoudj, D. Debarnot, B. Bêche, F. Poncin-Epaillard, Talanta 76 (2008) 314.
[9] H. Zhou, H. Chen, S. Luo, J. Chen, W. Wei, Y. Kuang, Biosens. Bioelectron. 20 (2005) 1305.
[10] K. Kamaraj, S. Sathiyanarayanan, G. Venkatachari, Prog. Org. Coat. 64 (2009) 67.
[11] J. Jiang, L. Li, M. Zhu, React. Funct. Polym. 68 (2008) 57.
[12] G. Li, S. Yan, E. Zhou, Y. Chen, Colloids Surf. A: Physicochem. Eng. Aspects 276 (2006) 40.
[13] Ö. Yavuz, M.K. Ram, M. Aldissi, P. Poddar, S. Hariharan, J. Mater. Chem. 15 (2005) 810.
[14] L.-H. Ai, J. Jiang, J. Alloys Compd. 487 (2009) 735.
[15] J. Jiang, L.-H. Ai, Mater. Lett. 62 (2008) 3643.
[16] L. Li, Ch. Xiang, X. Liang, B. Hao, Synth. Met. 160 (2010) 28.
[17] J. Jiang, L. Li, F. Xu, Mater. Sci. Eng. A 456 (2007) 300.
[18] J. Jiang, L.-H. Ai, D.-B. Qin, H. Liu, L.-C. Li, Synth. Met. 159 (2009) 695.
[19] J. Jiang, L.-H. Ai, L.-Y. Liu, Mater. Lett. 64 (2010) 888.
[20] T.-H. Ting, K.-H. Wu, J. Magn. Magn. Mater., in press.
[21] C. Yang, H. Li, D. Xiong, Z. Cao, React. Funct. Polym. 69 (2009) 137.
[22] X. Lu, H. Mao, D. Chao, W. Zhang, Y. Wei, J. Solid State Chem. 179 (2006) 2609.
[23] S. Ameen, M.S. Akhtar, G.-S. Kim, Y.S. Kim, O.-B. Yang, H.-S. Shin, J. Alloys Compd. 487 (2009) 382.
[24] B.K. Sharma, N. Khare, S.K. Dhawan, H.C. Gupta, J. Alloys Compd. 477 (2009) 370.
[25] L. Chen, L.-J. Sun, F. Luan, Y. Liang, Y. Li, X.-X. Liu, J. Power Sources 195 (2010) 3742.
[26] B.H. Kim, W.G. Hong, S.M. Lee, Y.J. Yun, H.Y. Yu, S.-Y. Oh, C.H. Kim, Y.Y. Kim, H.J. Kim, Int. J. Hydrogen Energy 35 (2010) 1300.
[27] A. Olad, B. Naseri, Prog. Org. Coat. 67 (2010) 233.
[28] B.C. Kim, J.S. Kwon, J.M. Ko, J.H. Park, C.O. Too, G.G. Wallace, Synth. Met. 160 (2010) 94.
[29] J. Yan, T. Wei, Z. Fan, W. Qian, M. Zhang, X. Shen, F. Wei, J. Power Sources 195 (2010) 3041.
[30] Q. Liu, M.H. Nayfeh, S.-T. Yau, J. Power Sources 195 (2010) 3956.
[31] H. Zhang, Q. Qi, D.G. Evans, X. Duan, J. Solid State Chem. 177 (2004) 772.
[32] X. Duan, Q.Z. Jiao, L. Li, Chinese Patent CN 99119385.7 (1999).
[33] X. Duan, Q.Z. Jiao, Chinese Patent CN 00132145.5 (2000).
[34] Y. Zhao, F. Li, R. Zhang, D.G. Evans, X. Duan, Chem. Mater. 14 (2002) 4286.
[35] X. He, Q.Z. Ling, Mater. Lett. 4284 (2002) 1.
[36] M.A. Ahmed, A.A. El-khawlani, J. Magn. Magn. Mater. 321 (2009) 1959.
[37] J.P. Pouget, M.E. Jozefowicz, A.J. Epstein, X. Tang, A.G. Macdiarmid, Macromolecules 24 (1991) 779.
[38] M.R. Karim, C.J. Lee, M.S. Lee, J. Appl. Polym. Sci. 103 (2007) 1973.
[39] L. Li, J. Jiang, F. Xu, Mater. Lett. 61 (2007) 1091.
[40] A. Goldman, Modern Ferrite Technology, Springer, 2006, 2nd ed., p. 58.
[41] R. Kaiser, G. Miskolczy, J. Appl. Phys. 41 (1970) 1064.
[42] K.H. Wu, Y.M. Shin, C.C. Yang, W.D. Ho, J.S. Hsuj, Polym. Sci.: Part A: Polym. Chem. 44 (2006) 2657.
[43] Y. Long, Z. Chen, J.L. Duvail, Z. Zhang, M. Wan, Physica B 370 (2005) 121.
[44] D. Mahanta, G. Madras, S. Radhakrishnan, S. Patil, J. Phys. Chem. B 112 (2008) 10153.
[45] D. Mahanta, G. Madras, S. Radhakrishnan, S. Patil, J. Phys. Chem. B 113 (2009) 2293.